JOURNAL OF AIRCRAFT
Vol. 42, No. 3, May–June 2005

Two Supersonic Business Aircraft Conceptual Designs, With and Without Sonic Boom Constraint

David C. Aronstein* and Kurt L. Schueler†
Raytheon Aircraft Company, Wichita, Kansas 67201-0085

A pair of supersonic business jet conceptual designs has been developed to assess the impact of designing for reduced sonic boom. One aircraft was designed without a sonic boom constraint. The other was limited to an initial sonic boom overpressure of 0.4 lb/ft^2. All other design requirements were the same. Sonic boom mitigation places a requirement on the buildup of lift and volume along the longitudinal axis of the aircraft, with any excess or shortfall adversely impacting the sonic boom. Methods were developed for incorporating this requirement into the conceptual design process. Both the method for incorporating the boom constraint in the design process and the result, a side-by-side comparison of one low-boom and one unconstrained aircraft with substantially identical performance in all other respects, are considered significant. The boom-constrained aircraft was approximately 25% longer with 18% higher takeoff gross weight than the unconstrained aircraft.

Nomenclature

A	=	area
$C_{D(\text{wave})}$	=	coefficient of wave drag due to volume
C_L	=	lift coefficient
C_M	=	pitching moment coefficient
D(wave)	=	wave drag due to volume
L	=	length
L/D	=	lift-to-drag ratio
l	=	lift (local)
M	=	Mach number
q	=	dynamic pressure
T/W	=	thrust-to-weight ratio
V	=	volume or velocity
W	=	weight
W/S	=	wing loading
X or x	=	longitudinal coordinate
β	=	factor $(M^2-1)^{1/2}$
η	=	normalized slope of ramped pressure rise
θ	=	orientation of Mach planes, 90 deg when planes cut down and aft
Λ	=	wing sweep angle

Subscripts

c.g.	=	center of gravity
e or equiv	=	equivalent, or in equivalent coordinates
ideal	=	pertaining to a theoretical ideal body of same length and volume
LE	=	leading edge
lift	=	due to lift
max	=	maximum
min	=	minimum
S	=	stall

Presented as Paper 2004-697 at the AIAA 42nd Aerospace Sciences Meeting and Exhibit, Reno, NV, 5–8 January 2004; received 14 January 2004; revision received 19 October 2004; accepted for publication 19 November 2004.

*Principal Aeronautical Engineer, Advanced Design Engineering. Senior Member AIAA.

†Senior Aeronautical Engineer, Advanced Design Engineering. Senior Member AIAA.

Introduction

RESEARCH has shown that a market for supersonic business aircraft exists,[1] with the ability to fly supersonically over land as a key requirement. However, current civil regulations do not permit supersonic flight in the continental United States, regardless of sonic boom signature. Specifically, Federal Aviation Regulation (FAR) 91.817 prohibits supersonic civil operations within the United States unless specifically authorized, as well as operations into or out of the United States in a way that would cause a sonic boom to reach the ground within the borders of the United States. Regulatory change is, therefore, a prerequisite to the successful operation of a supersonic business aircraft. Until such change occurs, supersonic business aircraft design studies can only proceed on the assumption that some sonic boom signature level will eventually be defined as acceptable.

The purpose of this study is to evaluate the impact of a sonic boom constraint by designing two aircraft to the same set of mission requirements, one having a constrained sonic boom signature and one having an unconstrained signature. For the present study, a boom signature with a maximum initial overpressure of 0.4 lb/ft^2 is assumed to be acceptable. A "hybrid" signature shape is used, with a short flat section followed by a ramped rise, as shown in Fig. 1. The flat section provides invariance of the initial overpressure to moderate changes in atmospheric temperature.[2] For comparison, Fig. 1 also shows the signature of a 125,000-lb aircraft flying at Mach 1.8 with no boom reduction, having an initial overpressure of approximately 1.25 lb/ft^2 with an N-wave form (an initial shock, followed by a nearly linear expansion to less than ambient pressure, followed by a tail shock that recovers to ambient pressure). The Concorde aircraft produces an N wave with an overpressure of approximately 2 lb/ft^2 (Ref. 3). Whereas this is only 0.1% of the ambient pressure at sea level (2116 lb/ft^2), it is still significant in terms of its impact to people, structures, and the environment. The target pressure rise is approximately one-third that of an unimproved supersonic business jet and one-fifth, that of the Concorde.

All design requirements used for the present study are summarized in Table 1. Table 2 lists the analysis tools that were used. This paper focuses on the integration of the sonic boom constraint with the design process and particularly with the issues of balance and volume management.

Historical Background: Sonic Boom Research

The study of sonic boom propagation began at approximately the same time as the beginning of supersonic flight. In 1947, Hayes published the relationships that enabled a complex aircraft configuration in supersonic flight to be replaced with an equivalent body of revolution.[10,11] Hayes's results are applicable to the calculation

Table 1 Design requirements

Parameter	Value
Range, nm, design mission	5000
Cruise speed, Mach	1.8
Takeoff field length, ft, sea level, standard day	6000
Outside cabin diameter, in.	$\geq$70
Payload (passengers)	
Maximum	8
Design mission	6
Airfield noise	FAR 36 stage 4
Initial overpressure, lb/ft^2, boom-constrained aircraft only	0.4
Signature shape, boom-constrained aircraft only	Flat top first 10% ramped rise, $\eta = 0.3$

Table 2 Analysis tools used

Task	Tool	Source	Comments
Boom	Darden[4]	NASA	Find minimum length for a given boom signature, weight, Mach, and altitude
Boom	HybridF^2	NASA	Generate equivalent area distribution
Boom	PBoom[5]	NASA	Evaluate sonic boom of actual configuration
Aero	Wingdes[6]	NASA	Design wing camber, evaluate drag due to lift
Aero	VORLAX[7]	NASA	Evaluate longitudinal lift distribution for boom
Aero	AWAVE[8]	NASA	Evaluate wave drag due to volume
Weight	FLOPS[9]	NASA	Weight buildup

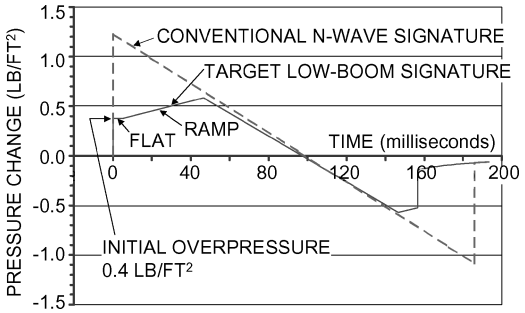

Fig. 1 Target sonic boom signature.

of both the wave drag and the sonic boom of a vehicle in supersonic flight. During the early 1950s, Witham developed a method of correcting the linearized theory for speed-of-sound gradients in the atmosphere.[12,13] These two contributions provided a basic system for predicting the sonic boom ground signatures of supersonic aircraft.

During the later 1950s and 1960s, there came a great number of theoretical advances, augmented with test data, that were becoming available from the increasing number of supersonic military aircraft. The effects of aircraft length, weight, and flight profile were well understood. There were further advances in the understanding of atmospheric effects, in the prediction of ground signatures at locations laterally displaced from the flight path, and in the understanding of the flow in the immediate vicinity of the aircraft, a regime not covered by the linearized aerodynamic methods. Computer techniques were developed for both near-field and far-field calculations. A complete review of these developments is beyond the scope of this paper; excellent reviews have already been published by Carlson and Maglieri,[14] and by Seebass.[15]

Three regions of signature development were identified: the near field, midfield, and far field. The near-field pressure signature is dominated by the detailed geometric features of the configuration. Linearized methods, which replace the detailed geometry with a body of revolution, cannot predict the near-field signature. In the midfield, the complex structures of the near-field coalesce into a simpler signature that is predictable by linear methods. With increasing distance from the flight path, further coalescence takes place, normally leading to an N wave in the far field. The actual extent of each regime is dependent on the configuration and the flight conditions.

All of the flight-test data taken during that period were limited to N-wave-type signatures. These were, and in general still are, the only signatures produced by any operational supersonic aircraft. Without careful attention to the shaping of the vehicle, and in particular to the lengthwise distributions of lift and volume, the shocks quickly coalesce into an N wave.

However, during the later 1960s, two important advances led to the possibility of aircraft with other types of signatures. First, it was realized that the midfield region can extend several hundred body lengths below the aircraft in a homogeneous atmosphere and indefinitely in a real atmosphere.[16,17] Thus, the ground signature need not be the far-field N wave. Second, based on this realization, several researchers performed signature minimization studies, minimizing parameters such as initial shock strength, peak overpressure, etc., for a given vehicle length and weight, or, alternatively, finding the minimum length for a given signature. Flat-top, ramped, and other signature shapes were explored. The most general and valuable work on minimization of its time was published by Seebass and George in 1972 (Ref. 18).

The area distributions required for sonic boom minimization, however, are not the same as those required for minimum wave drag. Specifically, sonic boom minimization requires a more rapid buildup of volume at the nose of the vehicle. This nose bluntness incurs a wave drag penalty. There were also challenges involved with making the combined lift and volume distributions of a practical design match the distribution required to produce a given boom signature. No attempts were yet made to apply sonic boom reduction theory to real aircraft.

The TU-144 and Concorde supersonic civil transport aircraft made their first flights in 1968 and 1969, respectively. The U.S. supersonic transport program was canceled in 1971. The Concorde entered commercial service in 1976. Rules were established prohibiting civil supersonic operations overland due to sonic boom. Military aircraft conducted supersonic operations in approved corridors. Space shuttle missions, starting in 1981, also involved supersonic flight over certain areas during a portion of the descent. The Concorde made its supersonic transatlantic passages, but there was little near-term prospect of any other supersonic civil aircraft.

Theoretical advances continued, however. In 1979 Darden published a method, with computer program, for minimizing either the initial shock strength or the absolute peak overpressure, while relaxing the extreme nose bluntness of the low-boom shapes developed previously.[4] An updated version of this computer code was used in the present study.

In the late 1980s, NASA and the U.S. commercial aircraft industry embarked on the high-speed civil transport (HSCT) and high-speed research (HSR) programs, which stimulated further research.[19] Two developments from this period were used directly in the present study. One is the hybrid signature, a practical signature shape that is predicted to be insensitive to moderate variations in atmospheric conditions.[2] This signature shape is an extension by Mack and Haglund[2] of the works of Darden and of Seebass referenced earlier. The other is an improved method of accounting for the nacelles in the equivalent area distribution, developed by Mack.[20]

However, the overall conclusion was that the signature of a roughly 750,000-lb aircraft could not be practically reduced to an acceptable level, and so there was little effort directed at sonic boom reduction in the HSCT/HSR program after 1994. Furthermore, in 1999, the HSR program was canceled entirely.

In 2000, the Defense Advanced Research Projects Agency (DARPA) launched the quiet supersonic platform (QSP) program, which provided renewed impetus for sonic boom research. Learning from the HSR experience, attention was now focused on a smaller class of aircraft, 100,000–125,000 lb takeoff weight, for

which it might be practical to reduce the initial shock strength to 0.5 lb/ft^2 or less. This program aimed for dual applicability: a military supersonic-cruise strike aircraft and a civil supersonic business jet. NASA and several commercial and general-aviation manufacturers have also conducted studies of supersonic business aircraft.

Recent technical advances include the increased use of computational fluid dynamics rather than linear theory to predict pressure signatures[3,21–23] and the shaped sonic boom demonstrator (SSBD) project, which is the first and, to date, the only flight-test validation of a shaped sonic boom signature.[24,25]

The QSP program stimulated various efforts to apply numerical optimization, including multidisciplinary optimization (MDO) techniques, to low-boom vehicles. At first these efforts were frustrated by the extreme sensitivity and highly nonlinear behavior of the boom signature with respect to small changes in the vehicle shape and/or lift distribution. However, researchers at Stanford University have achieved promising results by departing from the concept of a "designed" signature shape and using genetic algorithms to optimize the perceived noise level, rather than the initial or peak overpressure of the sonic boom signature.[26]

The Concorde aircraft produced an N wave with an overpressure of approximately 2 lb/ft^2. NASA HSR studies considered 0.8–1.0 lb/ft^2 to be low for an HSCT-class vehicle (approximately 750,000-lb takeoff weight).[19,27] A business jet class vehicle with 125,000-lb takeoff weight and no boom reduction would have an N-wave signature of 1.25 lb/ft^2. The DARPA QSP program had an initial goal of 0.3-lb/ft^2 initial pressure rise. Military activity, although continuing, appears to be focusing on less demanding boom reduction goals. Subsequent studies by NASA and commercial aircraft manufacturers have focused on the range of 0.4–0.7 lb/ft^2 (Refs. 1, 22, 28, 29).

Gulfstream,[28] Boeing,[29] and NASA Langley Research Center[30] have all presented what appear to be viable supersonic business aircraft designs having boom signatures in this range. Gulfstream has also published methods for nonaxisymmetric shaping that offer a slight improvement in boom signature, relative to what linear analysis methods would predict.[31]

One unique contribution of the present study is the presentation of two designs, one of which is low boom and one of which is not, having otherwise identical mission capabilities to within the accuracy of the methods used. This provides a direct measurement of the cost of the boom constraint in terms of vehicle size, weight, and other factors that may emerge as discriminators between the two aircraft. Another contribution is the presentation of a specific process for managing sonic boom design, at the linear-theory level, in conjunction with the other competing requirements of volume, wave drag, and balance.

Review of Linear Sonic Boom Concepts

Equivalent Area

Linear sonic boom theory is closely related to linear wave drag theory (the familiar area rule). It is based on representing the actual three-dimensional aircraft configuration with a linear distribution of disturbances along a reference axis. This distribution of disturbances can also be thought of as the equivalent body of revolution; the disturbances correspond to changes in the cross-sectional area. The cross-sectional area of the equivalent body is called the equivalent area.[14]

As is the case in wave drag calculation, the equivalent body is generated by cutting the configuration with Mach planes and then projecting the cuts onto normal planes before evaluating the areas. [Mach planes are those planes that make an angle of $\arcsin(1/M)$ with the direction of motion. The Mach angle refers to the angle between the Mach plane and the direction of motion; the azimuth angle refers to the roll angle of the Mach plane about the direction of motion.] The area of the streamtube taken into the propulsion system, measured upstream of any disturbance created by the aircraft, is normally excluded from the calculation.

There is a key difference between the equivalent body for wave drag and the equivalent body for sonic boom computation. A wave drag computation uses Mach planes oriented at all azimuth angles (or, practically, a reasonable number of equally spaced azimuth angles) and averages the resulting drag. A sonic boom computation only uses Mach planes of a particular orientation, specifically, the Mach planes that are tangent to the aircraft Mach cone on a line from the apex to the measurement point. In the most common case of measurement directly below the flight path, the Mach planes of interest cut down and aft, as shown in Fig. 2.

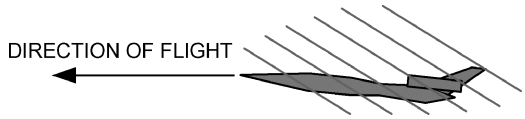

Fig. 2 Mach planes used for boom analysis.

Each cut is then projected onto a plane that is normal to the flight path, located at the station where the Mach plane intersects some longitudinal reference line. This reference line is called the equivalent x axis. The area of the projected cut is the equivalent area at this station. Whereas the equivalent area is not equal to the normal cross-sectional area, note that volume is preserved by the projection of the Mach plane cuts back to normal planes, and all volume of the configuration is accounted for exactly once. The integrated equivalent volume, not including lift contributions, is, therefore, equal to the total physical volume of a configuration.

The second key difference between the equivalent body for sonic boom, and the equivalent body for wave drag, is that the equivalent body for sonic boom analysis includes a lift contribution. Positive lift produces a positive pressure perturbation below the aircraft. To an observer below the flight path, lift, therefore, appears to be a positive area change. An observer directly to the side is unaffected by upward lift, and an observer directly above the flight path will experience a decrease in pressure after a lifting vehicle flies past; therefore, that observer sees lift as a negative area change. Mathematically, this is expressed as follows:

$$\frac{\mathrm{d}Ae_{\mathrm{lift}}}{\mathrm{d}x} = \left(\frac{\beta}{2q}\right) \times \sin\theta \times \frac{\mathrm{d}l}{\mathrm{d}x} \tag{1}$$

where Ae_{lift} is the equivalent area due to lift, β is the factor $(M^2-1)^{0.5}$, θ is the roll angle defined as 90 deg when the lift is vertically upward and the boom signature is being calculated directly below the flight path, and $\mathrm{d}l/\mathrm{d}x$ is the lift per unit equivalent length at a given station. Note that the equivalent area due to lift is cumulative: It is not the value of the equivalent area, but the rate of change of the equivalent area that is proportional to the local lift per unit length. As long as all of the lift is upward, equivalent area due to lift only increases over the length of a configuration. Regardless of whether or not all lift is upward, at $x = L_{\mathrm{equiv}}$, the equivalent area due to lift has the final value:

$$Ae_{\mathrm{lift}} = W\beta/2q \tag{2}$$

where L_{equiv} is the equivalent length of the vehicle and W is the weight, which is equal to the total lift in steady level flight.

As suggested by the foregoing discussion, these methods are not restricted to calculations directly below the flight path, although bending of rays becomes important at large lateral displacements, and, in fact, there will normally exist a maximum lateral displacement beyond which no boom signature reaches the ground. However, it is possible that at some distance off center, the boom signature may be more severe by some measure(s) than it is directly below the flight path. It is also likely that the boom signature in some part(s) of the climb or descent profile may be more severe than the boom signature in cruise. Turns, climb, descent, acceleration, and deceleration can all affect the boom footprint on the ground. Boom calculations in the present study were limited to cruise conditions and to locations directly below the flight path, but it is recognized that a more thorough investigation would be required as the design evolution continues.

Target Equivalent Area Distribution

Linear sonic boom theory uses the equivalent area distribution to calculate a quantity known as Whitham's[12,13] F-function, and

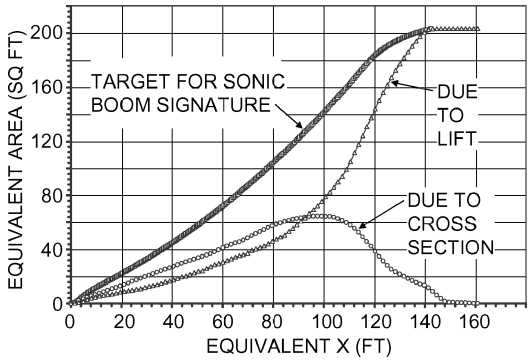

Fig. 3 Typical equivalent area distribution.

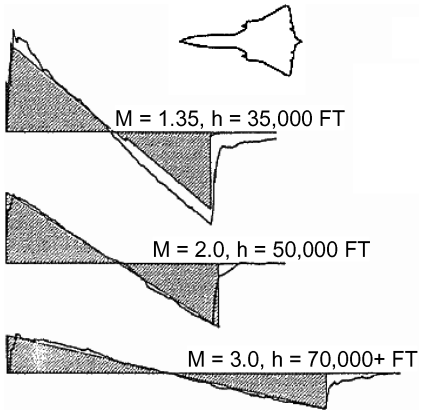

Fig. 4 Theory to flight-test comparison (Ref. 14): ——, flight data and ▨, theory.

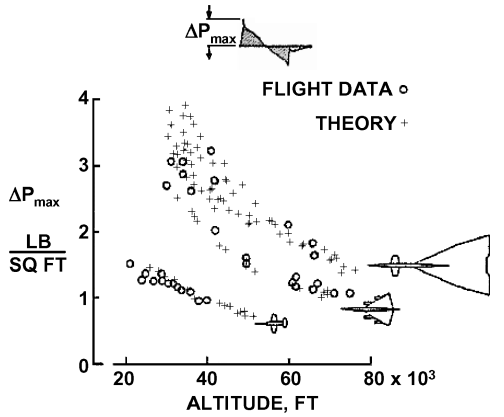

Fig. 5 Flight data, various aircraft.[14]

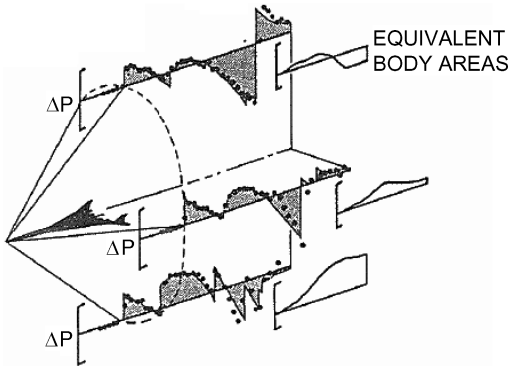

Fig. 6 Theory to wind-tunnel comparison (Ref. 14): $M = 1.4$, $h/l = 2.5$; ●, Experiment and ▨, theory.

uses the F-function to calculate the propagated boom signature. The development of the equations can be found in Refs. 4, 14, and 18 and will not be repeated here. The relationship is complex, and there is no convenient system, short of repeating the boom analysis, for determining what effect a given change in the equivalent area distribution will have on the boom signature.

Of particular interest, however, is that one may start with the desired boom signature, together with the aircraft's weight, cruising altitude, and Mach number, and derive the equivalent area distribution that will produce the desired signature. The method of Seebass and George,[18] as extended by Darden[4] and by Mack and Haglund,[2] make this possible for a variety of useful signature forms. The designer's problem is simplified; one need not be concerned with the boom signatures produced by the various features of the aircraft, but only with making sure that the entire configuration conforms to the required equivalent area distribution. This process also tells the designer what the minimum equivalent length of the vehicle must be.

A typical target equivalent area distribution is shown in Fig. 3. The cross section and lift contributions may be traded off against each other as long as the total distribution matches the target.

Validation of Linear Theory

Flight tests conducted in the 1960s provided extensive validation of the accuracy of the linear theories and atmospheric propagation models, at least insofar as predicting the strength and duration of the N-wave signatures for various aircraft at various weights and flight conditions.[32–35] Samples of such data are shown in Figs. 4 and 5. Figure 4 shows good agreement of both the strength and the duration of the signature except at a Mach number of 1.35. Other sources also note reduced accuracy of linear methods at Mach numbers below 1.4 (Ref. 5).

Figure 5 shows data from an extensive body of tests at a variety of weights, altitudes, and Mach numbers. The data band for each aircraft represents all weights and Mach numbers flown by that aircraft at that altitude. Whereas the data shown do not permit correlation of specific weights and Mach numbers, the overall agreement is quite good: The theory bands overlay the flight data bands almost exactly.

A comparison of theory to wind-tunnel data is shown in Fig. 6. As in Fig. 4, the agreement is quite good. In this case, the agreement is demonstrated not just for an N wave, but for the more complex signature that exists at a distance of 2.5 body lengths from the flight path. It is noted in Ref. 14 that the good agreement with linear theory may be misleading at such small distances from the flight path, but the accuracy of the theories at distances corresponding to normal flight altitudes, and at Mach numbers between 1.4 and 3.0, is generally accepted.

However, each type of test has always been limited by certain factors. Flight data were limited to N-wave signatures because that is what all supersonic aircraft have produced before 2003. Wind-tunnel tests, on the other hand, have been used to validate shaped signatures, but only to a relatively small number of body lengths away from the vehicle and only in the essentially homogeneous atmosphere of the wind tunnel. There remains the uncertainty regarding the persistence of shaped signatures to the ground in the real atmosphere.

The SSBD project has provided the first opportunity to validate a shaped sonic boom signature prediction with flight data. Detailed analyses of the SSBD results have not been published yet, though they are expected soon. There were a small number of runs that produced usable data during the initial series of flights in August 2003, and a much more extensive set of data was obtained during follow-up tests in January 2004. The limited data that have been published, from the 2003 tests, show good agreement with predictions. The SSBD tests were conducted by Northrop Grumman, DARPA, and NASA, as part of DARPA's QSP program.[24]

The present study utilized the Darden[4] and HybridF[2] codes to design the low boom area distributions and PBoom to analyze the signature of a completed configuration. Also, the wave drag calculations in this study were performed using AWAVE,[8] a version of the Harris program that has been modernized at NASA for computing performance, but that still utilizes the original theory and

equations. These codes are all published by NASA; the referenced reports include validation data. They are in current use in NASA and industry and are accepted as accurate implementations of the linear aerodynamic theory.

Design Implications

The target equivalent area distribution is an exact requirement in the sense that a deviation below the target distribution may be as harmful as a deviation above the target. The impact of a deviation is a function of its abruptness and its magnitude. The location of a deviation also influences how strong the effect will be and determines which part of the signature it will affect. Generally, deviations forward of the main inflection point (the curvature change that is seen slightly to the left of 120 ft in Fig. 3) affect the forward features of the boom signature, whereas deviations after the inflection point will affect the tail shock. Deviations that are sufficiently small and smooth may be acceptable, but there is no simple rule that tells the designer whether this will be the case.

In the preliminary design, it is, therefore, necessary 1) to treat the target equivalent area distribution with sufficient priority to ensure that it is met and 2) to provide realistic volume allocations so that bulges and bumps will not have to be added later.

All supersonic configurations require careful volume management to minimize wave drag while providing adequate volume for fuel, structure, systems, and payload. A sonic boom constraint adds the following fundamental challenges:

1) The minimum length to meet a boom constraint is usually quite long, imposing a weight penalty.

2) The increased length is not accompanied by a wave drag savings, and, in fact, there may be a wave drag penalty because the area distribution for boom is not optimum for wave drag. Specifically, low boom usually requires a blunter nose than is optimum for wave drag.

3) There may be difficulty fitting the vehicle structure, systems, fuel, and/or payload within the equivalent area target. Violation of the boom signature, reductions in accommodation, and/or failure to integrate the design may result.

4) There may be difficulty in achieving longitudinal balance. There is a fundamental tradeoff between the lift and cross section contributions to the equivalent area, which is discussed in the following section. If this relationship is not recognized and treated properly in the very early stages of a design, it can lead to a configuration that cannot be balanced except by violating the boom constraint.

Balance and Volume Management Tradeoff

The equivalent area chart plots equivalent cross-sectional area against equivalent length, so that plot area on the chart corresponds to equivalent volume of the configuration. The total equivalent volume of a configuration, including physical volume plus equivalent volume due to lift, is equal to the plotted area under the overall target curve. The physical volume available is, therefore, equal to the area under the overall target, minus the area under the lift curve.

The area under the lift curve may be analyzed as shown in Fig. 7. The area of a horizontal "slice" under the lift curve is equal to the incremental growth in Ae due to lift times the distance from the

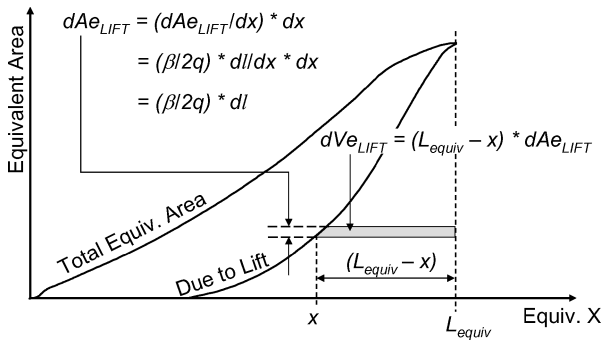

Fig. 7 Equivalent volume due to lift.

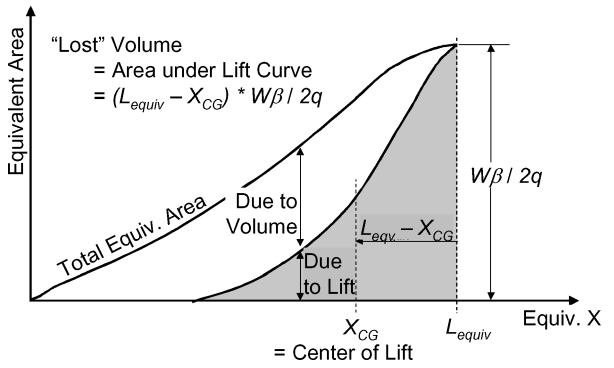

Fig. 8 Balance to volume tradeoff.

point at which the lift is generated to the aft end of the vehicle. Substituting the second expression for dAe_{lift} into the expression for dVe_{lift} and integrating yields the following:

$$Ve_{\text{lift}} = (\beta/2q) \times W \times (L_{\text{equiv}} - X_{\text{lift}}) \tag{3}$$

where Ve_{lift} is the equivalent volume due to lift, X_{lift} is the center of lift that must be the same as the center of gravity, and all other terms are as already defined. The lost volume due to lift is, therefore, directly linked to the c.g. location.

This tradeoff between the c.g. location and the available physical volume remaining is shown in Fig. 8. Altering the lift distribution to move center of lift forward (to the left, in Fig. 8) will require an increase in the equivalent volume due to lift (shaded) and reduce the remaining physical volume available. Moving the center of lift aft will increase the physical volume, but it may not be possible to utilize it all while maintaining the c.g. at the center of lift.

Two caveats must be kept in mind. First, although it is possible to use pitch control surfaces to trim about a range of c.g. locations, this will affect the equivalent area distribution. A trim download at the aft end must be compensated by additional lift elsewhere, so that the total lift is still equal to the weight. Therefore, any trim loads must be included in the design equivalent lift distribution. Control deflection cannot be used to compensate for a failure to balance the configuration in the preliminary stages.

Second, all of the foregoing discussion refers to the equivalent x axis, not the body x axis. Vertical displacement of lift or weight alters the relationship between equivalent x and physical x. All discussion relating physical balance to equivalent area distributions is, therefore, approximate. A high-wing configuration will have the center of lift farther forward in physical coordinates than a low-wing configuration with the same equivalent lift distribution. Nevertheless, the c.g. and the center of lift must be close to each other on the equivalent axis to have any possibility of being at the same physical x location. If the vertical locations of the center of lift and of the c.g. are known or estimated, then both can be translated into body axes, and the error of this approximation can be eliminated. This correction was made in the present study.

It is necessary to ensure, very early in the design process, that the available volume distribution allows sufficient space for all internal items, with a c.g. location that is at the center of lift. It is not permissible, as on other aircraft, to define a preliminary configuration and then slide the wing fore or aft to achieve balance. Neither is it permissible to add local bulges in the fuselage contour to accommodate internal items.

Thus, it is important, while the wing planform and camber, wing location, and fuselage area ruling are being defined, to have a balance estimate that at least reflects the weight of each major internal or external weight item close to its correct location. It is also necessary to verify that the fuselage area ruling provides adequate volume for each major internal item in a location consistent with the balance calculation.

In a conventional design process, the arrangement of internal items is usually not treated until there is a full three-dimensional

CAD model of the configuration. The present study required fairly rapid development of a viable, aerodynamically efficient boom-constrained configuration. Linear aerodynamic methods were used to define the gross geometric and aerodynamic characteristics. To include three-dimensional internal layout work in each iteration of the design would be excessively slow and cumbersome. Specifically, the cycle time would have been increased by an order of magnitude.

Therefore, it was necessary to simplify the process for developing the internal layout, while retaining enough fidelity for c.g. estimation and volume verification. The problem was reduced to two dimensions and embedded in the postprocessing of the linear sonic boom analysis so that the impact on design cycle time was on the order of 20%.

Design Approach

Balance and Volume Management

The information available as inputs to the volume management and balancing process consisted of sizing data, the outputs of the aerodynamic analysis including the cruise center of lift location, and the outer-mold-line (OML) volume distributions of the major airframe components (wing, fuselage, empennage, and nacelles). The simplified method can be summarized as follows:

1) Describe the aircraft in terms of its major airframe components (wing, fuselage, empennage, and nacelles) and a manageable number of major internal items.

2) Describe the weight of each external and internal item in terms of known quantities such as maximum takeoff weight (MTOW), mission fuel weight, and wing area.

3) Describe the volume of each internal item in two dimensions, that is, a cross-sectional area and a length, or a cross-sectional area distribution.

4) Assign a c.g. to each external and internal item.

5) Use a tool that permits the user to manipulate the internal arrangement rapidly and to monitor compliance with requirements.

A fuel management system was assumed, so that the c.g. could be controlled within a range that was bounded by the forwardmost and aftmost fuel loading at a given weight. A fly-by-wire control system was also assumed, offering the opportunity to incorporate stability augmentation. It was, in fact, assumed that stability augmentation would be used to meet the applicable handling qualities requirements in all of the vehicle's flight regimes, whether or not it was statically stable. However, the maximum unstable margin was limited to 5% of the mean aerodynamic chord to avoid placing excessive demands on the performance and sophistication of the stability augmentation system.

Requirements on the internal layout were as follows:

1) All items must fit within available fuselage volume.

2) There must be sufficient volume for full fuel.

3) No fuselage fuel forward of the aft cabin bulkhead is permitted.

4) It must be possible to place the c.g. at the cruise center of lift, at all weights from start of cruise to end of cruise.

5) c.g. location that is stable, or no more than 5% unstable, must be attainable at all weights in subsonic and supersonic flight.

The weight of each major external component (wing, fuselage, nacelles, and vertical tail) was estimated by simple preliminary design methods.[36,37] The c.g. of each item was placed at its centroid of volume, except for the nacelle (including engine, nozzle, and engine-mounted accessories), which was placed at two-thirds of the nacelle length based on a preliminary layout of the nacelle. Because the locations and volume distributions of these items were already being used for the sonic boom calculation, the information was readily available for this analysis. It was necessary to add a Mach 1 analysis case at 0-deg angle of attack to the boom analysis, to generate a set of normal-cut area distributions.

Internal items of fixed shape were described in two dimensions by a cross-sectional area and a length. Fuel was assumed to fill available volume in appropriate sections of the wing and fuselage, subject to a structural allowance of 15% in the wing and 17% in the fuselage, along with an allowance of 0.6% for unusable fuel.[38] The rules developed for defining the internal arrangement are summarized in Table 3.

The rules for wing fuel were determined by analyzing the volume of a variety of swept wings. Fuel was located between 18 and 65% chord and from side-of-body to 60% semispan. It was found to be a good approximation that this region encompassed 45% of the total wing volume and that the centroid of the fuel volume was very close to the centroid of the total wing volume. This rule was, therefore, implemented, eliminating the need for a detailed fuel calculation on each candidate wing planform.

There was no explicit volume allocation for the flight-control system. Centralized flight-control components were considered to be included in the crew station, avionics, and hydraulic/electrical bays. The actuators themselves are located in the wing and tail surfaces. The weights of the surface controls were, therefore, allocated to the wing and empennage.

A standard nacelle was designed around the baseline engine to provide adequate volume for the engine and all engine-mounted accessories. This was scaled with the engine during sizing to meet the thrust requirements of the aircraft. Capture area was subtracted out for the purposes of sonic boom and wave drag calculation. This is the cross-sectional area of the airstream that is taken in to the

Table 3 Volume allocation rules for internal items

Item	Weight, lb	Cross section, ft^2	Length, ft	Volume, ft^3
Landing gear (nose)	900	7.0	7.8	55
Landing gear (main)	3320	21.9	11.7	257
Forward avionics plus crew station plus galley	1363 (including crew)	20.0 (average, some taper allowed)	10.9	218
Cabin plus lavatory plus aft avionics	1912	26.8	22.8	611
Passengers	1200[a]	Included in cabin		
Baggage external to cabin	800[a]	As required to provide 100 ft^3		100
Environmental control system (ECS)	342	15.0	2.0	30
Hydraulics, electrical	3088	15.0	8.0	120
Auxiliary power unit (APU) plus airframe-mounted engine accessories	420	As required to provide 90 ft^3	in aft end of fuselage	90
Routing for cables, ducts, etc.	Included in various sub-systems	1.8	Aft end of nose gear bay to forward end of accessories section	1.8 ft^2 × length
Usable fuselage fuel	Volume × 50.25 lb/ft^3	As available, less 17% of local fuselage cross section for structure	User input, must be aft of passenger cabin	Integrated from length and area, less 0.6% unusable
Usable wing fuel	Volume × 50.25 lb/ft^3	N/A	N/A	0.994 × 0.85 × 0.45 × OML volume of wing
Unusable fuel	0.6% of total fuel			

[a]Total payload is 1200 lb. Worst-case distribution between cabin and baggage used for each c.g. limit.

propulsion system, measured upstream of any disturbance created by the aircraft. It was not included in the boom and wave drag calculations because it does not flow around the aircraft; it flows through the aircraft. The nacelle area minus the capture area was considered to be the correct measure of the external disturbance of the airflow by the nacelle.

Weights shown in Table 3 represent the final low-boom aircraft configuration. During design, the weights were based on simple relationships. Many subsystem weights were treated as constant, whereas others were related to MTOW, wing area, or other high-level aircraft data available from the sizing. As the project progressed and a more thorough component weight buildup was developed, more accurate weight estimates were incorporated into the balance calculation.

The internal layout and balance calculations were embedded in a spreadsheet that was already being used to postprocess and view the results of the sonic boom analysis. Two plots were added: 1) a plot of the internal fuselage volume allocation and 2) a c.g. plot showing the cruise center of lift, the initial and final cruise weights, and the attainable range of c.g. location as a function of weight.

This made it a simple process to input the x axis locations of the major internal items and to check for fit, fuel volume, and balance. The most influential variables were the location of the main cabin and the start- and endpoints of the fuselage fuel. It was usually possible by manipulation of these three variables to determine whether or not a configuration was viable quickly.

The steps for volume allocation and balancing are represented in Figs. 9 and 10. Figure 9 shows the fuselage volume allocation, or slug chart, whereby the internal items were fitted into the area-ruled fuselage. Figure 10 shows the resulting c.g. for the same configuration, which is the final low-boom configuration of this study. Note again that the forward and aft loading lines do not represent actual c.g. travel. Rather, they represent the attainable c.g. range. The c.g. can be placed anywhere within the range shown through fuel management.

Design Integration and Iteration Process

The integration of the balance and volume management tasks with the rest of the design process is shown in Fig. 11. Outputs are shown below each step. First, the mission sizing sets the gross weight and

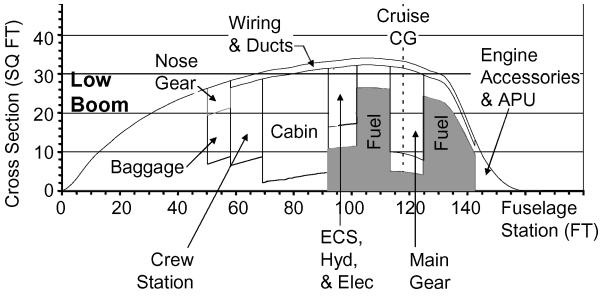

Fig. 9 Fuselage volume utilization.

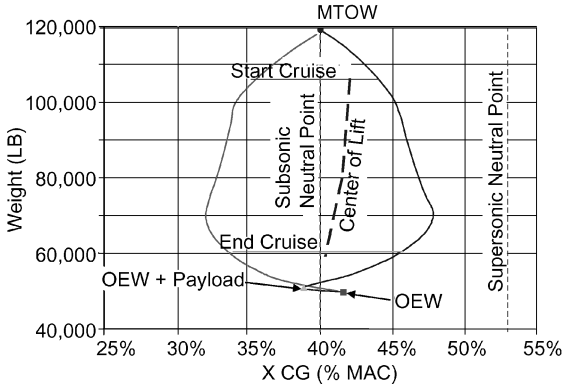

Fig. 10 Diagram, c.g.

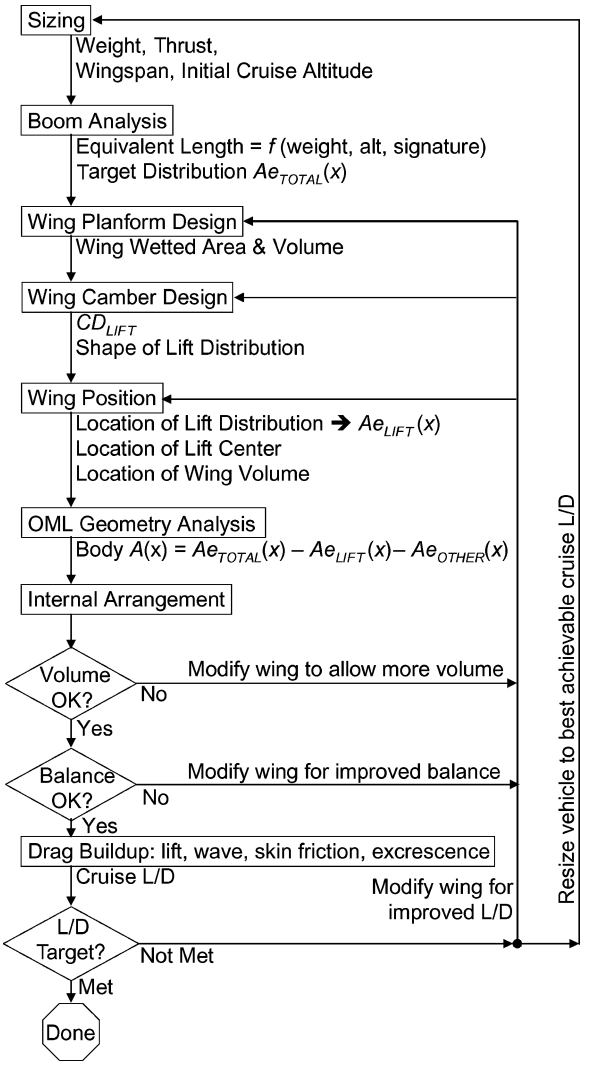

Fig. 11 Design process flowchart.

empty weight, thrust, wingspan, and cruise altitude based on an assumed cruise L/D. Given the initial cruise weight and altitude (and, of course, Mach number) and the desired boom signature, the HybridF and/or Darden codes provide the required length and the required equivalent area distribution. A wing planform is selected that, in combination with the selected thickness distributions, sets the shape of the wing volume distribution.

Wing camber design was performed next. WINGDES allows a user to specify C_M, or to select optimization regardless of C_M. It is always good to know what the overall optimum is, and so a family of cambers was usually designed for each wing planform: one with C_M unconstrained, and then several with C_M varying until the drag began to increase appreciably. Practical designs had C_M less positive than the unconstrained optimum (center of lift farther aft). It was usually possible to place the center of lift 5–10 ft aft of the unconstrained optimum and yet be within one drag count (0.0001) of the optimum design.

Once designed, the wing placement set the actual center of lift location and lift distribution with respect to the aircraft. All equivalent areas due to the wing were now known (volume and lift). Under the assumption that the other airframe components' volumes and locations were also known, that is, the vertical tail and the nacelle, the fuselage got the remainder. PBoom performed this step, as well as the subsequent analysis to verify that the resulting geometry produced the intended boom signature.

With the fuselage area distribution determined, it was then possible, using the approach of the preceding section, to stuff the internals and evaluate volume and balance. If volume was locally

inadequate, small planform changes could create local reductions in lift, with corresponding local increases in the available volume. If volume was generally inadequate, larger changes were required, as described hereafter.

In all cases, the changes were initiated with the wing, and the fuselage areas were allowed to adjust so that the target overall equivalent area distribution was maintained. In this way, every configuration implicitly met the boom requirement to the accuracy of the analysis method. This principle was adhered to whether the change was for volume, as discussed earlier, or for any of the other reasons that follow.

Under the assumption that the required items could be fitted into the configuration in some manner, the next check was balance. This is the point at which low-boom design becomes dramatically different from traditional subsonic or supersonic design. Attempting to address a nose-heavy condition simply by moving the wing forward usually made the condition worse. This is because, as noted earlier, any forward move of the center of lift was accompanied by a net reduction in volume, which typically forced items located in the aft end of the vehicle to move forward. The wing was chasing a moving target. Instead, it proved more effective to use changes in the lift distribution to drive changes in the fuselage area ruling, to allow a favorable shift of the internal arrangement.

Once fit and balance were achieved, a drag buildup was calculated, and the performance was checked. If there was a shortfall several options could be pursued. Wing planform and/or camber changes could be made to 1) reduce the drag due to lift, 2) reduce the wing wetted area, and/or 3) modify the lift distribution to drive a favorable change in area distributions for wave drag. In the third case, note that the change is, as always, initiated with the wing, even though the primary goal is to improve the area distribution of the fuselage. The final recourse was to iterate the sizing, updating the assumed cruise L/D to match the best values actually achieved in the analysis cycle.

The process was not completely automated. A moderate amount of human involvement was desirable in any case for monitoring of the progress as various issues were identified and addressed. Turnaround time was typically on the order of 2–4 work hours per design iteration (one pass through most of the steps shown). Optimization was performed within certain individual steps, but the configuration as a whole is not claimed to be "optimum." Rather, the final designs of this study are considered to be suitable starting points for MDO exercises.

Low-Speed Performance

The low-speed analysis problem was greatly simplified by it being the increase of induced drag, not the loss of lift that limits low-speed performance of highly swept low-aspect-ratio designs. When the precedent of the Concorde was followed, a minimum flight speed $V_{\min}$ was defined in lieu of a stall speed.[39] $V_{\min}$ was dictated by meeting the most critical of the climb gradient requirements of FAR 25.119 and 25.121, in the configuration and at the speed factor appropriate to each requirement.

Induced drag was evaluated using a low Oswald efficiency factor of 0.53, to reflect that highly swept wings at high lift do not come close to the full theoretical leading-edge thrust or suction that unswept wings with fully attached flow can achieve. This estimate includes a beneficial increment from plain drooped leading-edge flaps on the outboard wing. Other high-lift devices could include positive C_M devices (to improve the trimmed lift curve by allowing more trailing-edge-down elevon deflection) and/or devices to mitigate any unfavorable flow phenomena that might be found when a particular configuration reaches the stage of detailed aerodynamic investigation. These were not explicitly accounted for in the present study except in the form of a weight allowance. Landing gear and engine wind milling drag were included where appropriate, but had little significance compared to the induced drag. FAR 25.121(a), 0.0% gradient at liftoff speed, or FAR 25.121(b), 2.4% gradient at obstacle clearance speed, was always critical. FAR 25.121(c), en route configuration; FAR 25.121(d), approach climb; or FAR 25.119, landing climb, were never critical.

This method produced the interesting result that the effective $C_{L(\max)}$ varied from as little as 0.4 to as much as 0.9 among the configurations considered in this study, depending on aspect ratio, wing loading, and thrust loading. Nevertheless, these results justified the method because in all cases they confirmed that the usable C_L, as limited by climb gradient requirements, was achievable without any exotic high-lift devices. Also, in all cases, the liftoff C_L was achievable at a reasonable angle of attack (12 deg or less) based on estimates of the trimmed low-speed lift curves using appropriate and achievable c.g. locations.

Equation 5-91 of Ref. 36 was used for preliminary prediction of balanced field length, or rather, for enforcing that every configuration considered would meet the 6000-ft balanced field length requirement as closely as possible. Specifically, a tolerance band of $+0/-100$ ft was used. The equation predicts balanced field length as a function of wing loading, thrust loading, and lift coefficient at obstacle height, which was inferred from the $C_{L(\max)}$ value found as just described.

This equation was incorporated in the sizing, so that every design iteration by definition met the field length requirements through the selection and matching of thrust and wingspan, before any of the more detailed geometry characteristics of the wing planform and body areas were defined. Wingspan, rather than area, was treated as the almost-sacred quantity, consistent with induced drag, rather than aerodynamic stall in the conventional sense, being the limiting factor on usable lift. This was one of several areas in which rapid progress was facilitated by making the design process conform to the physics of the problem.

As soon as each configuration was defined in sufficient detail, a time-stepping calculation was performed as a check on the predicted field performance. The time-stepping calculation and the one-line equation generally agreed with each other to within 100 ft. However, it is recognized that the actual uncertainty is greater than that, due to the difficulty of accurately predicting the drag of highly swept wings at high lift and in ground effect.

Checks were also made to ensure that landing field length also did not exceed 6,000 ft. In every case, the predicted landing field length was less than the takeoff field length.

Airfield Noise

Airfield noise was estimated in accordance with FAA Advisory Circular AC 36-4C (Ref. 40). Airfield noise was treated in this study primarily as a driver for engine technology. Secondary effects on noise included airframe noise and airframe shielding of the engines. Both the low-boom and high-boom airframes were predicted to be relatively quiet because they lack the complex, multislotted high-lift systems that are a primary source of airframe noise on subsonic transport aircraft. In terms of shielding, the high and aft engine locations allowed the wings of both aircraft to provide significant shielding of the inlets at all noise measurement points (sideline, cutback, and approach). Both aircraft were predicted to meet the noise requirement, but the analysis cannot be discussed in detail herein because it involves data that are proprietary to the engine manufacturer.

Design Evolution

Initial low-boom configurations had the typical characteristics of an area-ruled fuselage with a waist at the wing and the passenger cabin located in the larger section forward of the wing.

The two most prevalent difficulties were 1) insufficient fuel volume aft of the passenger cabin and 2) inability to place the c.g. far enough aft at start of cruise.

To try to address these conditions, the relatively low-density passenger cabin was pushed as far forward as possible, with the lift beginning as soon as possible thereafter. This approach is shown in Fig. 12. However, this tended to exaggerate the area ruling of the fuselage. When a balanced configuration was finally achieved, it had an absurdly thin waist followed by a large bulbous region aft where most of the fuel was located. The main landing gear was located in the waist region, where there was not adequate volume for the gear bay.

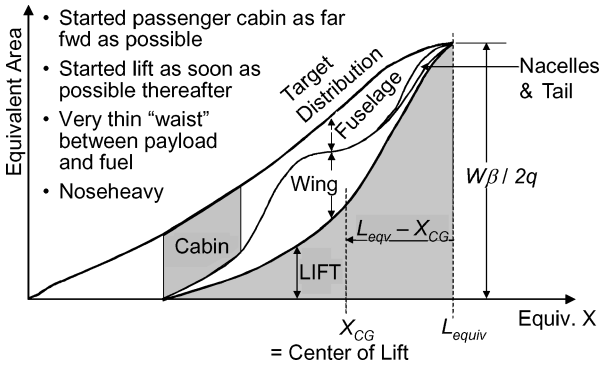

Fig. 12 Early low-boom design trends.

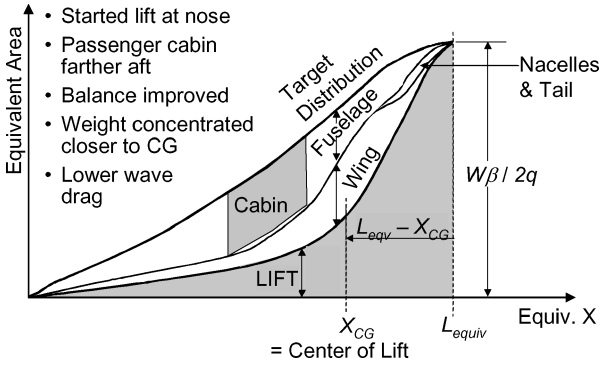

Fig. 13 Alternative approach to low-boom design.

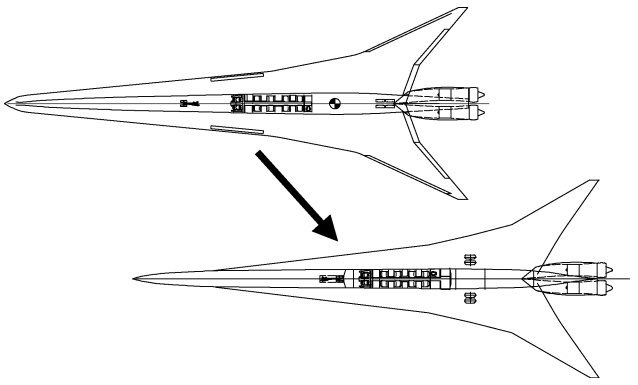

Fig. 14 Wetted area reduction.

A new approach was then tried, which is shown in Fig. 13. The inboard wing leading edge was extended forward to the nose, so that the lift began immediately. The passenger cabin had to move aft because the lift, as well as the physical volume of the wing, took up some of the equivalent area forward. However, the thin waist was eliminated, thereby recovering adequate volume for fuel and improving the prospects for successful integration of structure and main landing gear. The new configurations had better balance, with a much more centralized mass distribution.

The primary drawback of the new approach was high wetted area of the wing, due to the long leading-edge extension or strake. As weight and balance estimates were refined, it was found that the lift did not have to extend all of the way to the nose. Shortening the lift distribution slightly allowed the strake length, and wetted area, to be reduced. This progression is shown in Fig. 14.

As more refined analysis was conducted, various factors in the sizing method were updated to keep the sizing consistent with the latest analysis. This helped to keep the designs on target with respect to the mission performance requirements and to ensure a fair comparison between the boom-constrained and unconstrained designs.

Design Results

General Characteristics

The final constrained and unconstrained designs are summarized hereafter. By the use of the processes described herein, both designs met the mission performance requirements to within the accuracies of the methods used. This was necessary to ensure the validity of the comparison; neither design has any identified excess or shortfall of performance.

Specifically, tolerance bands of 100 nmile in range and 100 ft in field length were allowed on the favorable side of each respective requirement. Thus, both designs have a predicted range between 5000 and 5100 nmile and a predicted field length between 5900 and 6000 ft. Any variation within these bands was not considered significant in view of the accuracy of the methods used at this early stage of the design process.

Three views of both designs are presented to the same scale in Fig. 15. Table 4 summarizes the basic characteristics of the two designs.

The most apparent difference between the designs is the increased length of the low-boom configuration. As noted elsewhere, this takes

Table 4 Basic design characteristics

Characteristic	Low-Boom (constrained)	High-Boom (unconstrained)
MTOW, lb	119,200	101,400
Wing area, ft^2	2,743	1,770
Wingspan, ft	69.0	63.0
Aircraft length, ft	165.5	133.5
W/S, lb/ft^2	43.5	57.3
T/W	0.426	0.433
Operating empty weight (OEW)/MTOW	0.413	0.417
Fuel/MTOW	0.577	0.571
Thrust, lb	50,800	43,900
OEW, lb	49,200	42,200
Fuel weight, lb	68,800	57,900
Wing aspect ratio	1.74	2.24
Outboard Λ_{LE}, deg	60.0	60.0
Wetted area, ft^2	7,879	5,510
Volume, ft^3	6,030	4,500
Average cruise C_L	0.091	0.126
Average cruise L/D	7.95	8.23

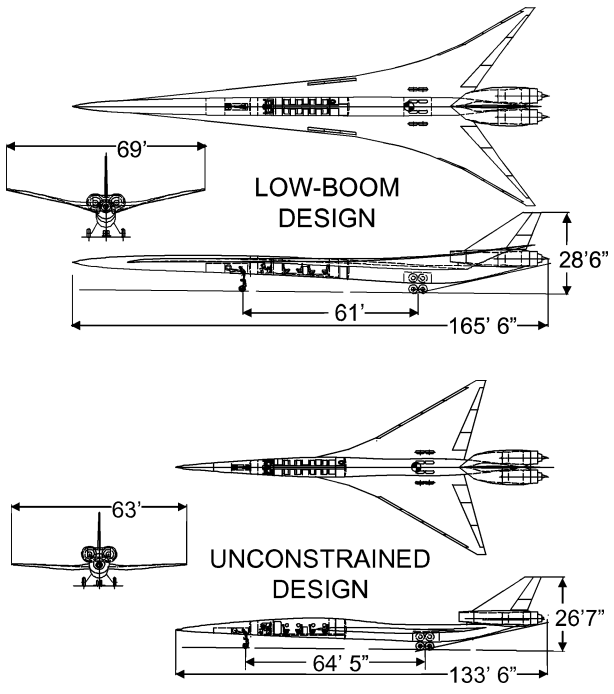

Fig. 15 Three views of low-boom and unconstrained designs.

the form of a forward extension of the nose and a lengthwise stretching of the wing. The additional volume in the nose is largely empty and, therefore, can be thought of as an aerodynamic fairing that exists for the purpose of tailoring the boom signature. Second, the low-boom configuration is generally larger in terms of wingspan, weight, thrust, etc., reflecting the impact of upsizing to achieve the same mission performance with the added weight and drag of the extended nose section. Third, the low-boom configuration has a significant amount of dihedral that is absent in the unconstrained design. Elevating the outboard wing in this manner causes its lift contribution to fall further aft on the equivalent x axis, or, conversely, allows a given equivalent lift distribution to be achieved with less sweep than would be required otherwise.

Balance and Volume

The internal arrangements are shown in Fig. 16. The two aircraft are seen to be similar in the relationship of internal items to each other and in their location with respect to the center of lift at the initial cruise condition. They carry similar quantities of fuselage fuel. The primary distinction is the large additional length and unused volume in the nose of the low-boom aircraft. The balance constraint precludes the use of this volume for heavy subsystems or useful load; it is essentially an empty aerodynamic fairing for sonic boom suppression.

Figures 17 and 18 show the c.g. diagrams of the low-boom and unconstrained aircraft, respectively. Both designs meet all balance requirements. The supersonic center of lift is within the attainable c.g. range shown at all weights from start of cruise to end of cruise. The stability requirement was to be stable, or no more than 5% unstable. Both configurations are stable in supersonic flight at all weights (c.g. ahead of the neutral point). The low-boom aircraft is

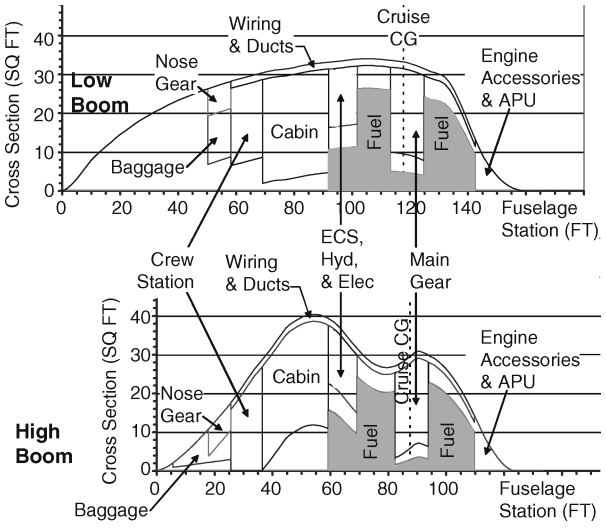

Fig. 16 Internal arrangements of final designs.

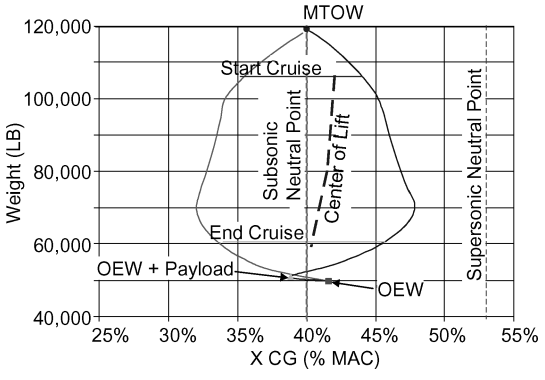

Fig. 17 Low-boom c.g. diagram.

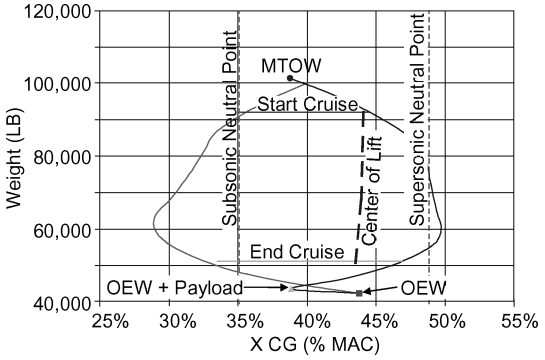

Fig. 18 High-boom c.g. diagram.

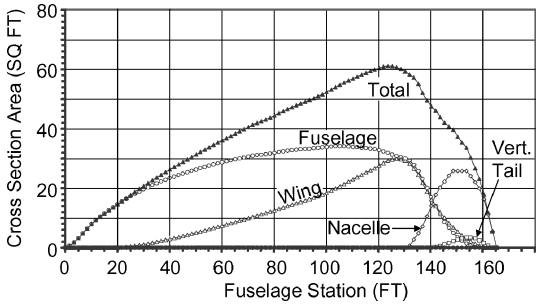

Fig. 19 Low-boom component area buildup.

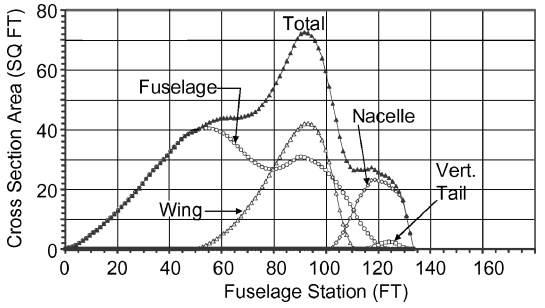

Fig. 20 High-boom component area buildup.

capable of maintaining neutral stability (c.g. at the neutral point), and the unconstrained aircraft is capable of maintaining $\leq$5% unstable margin in subsonic flight at all weights except with very low fuel and less than full payload. In this condition the low-boom aircraft may be up to 2% unstable, which is considered acceptable. The unconstrained aircraft, however, would become excessively unstable. Some redesign and/or flight limitations would be required for the unconstrained aircraft to address this very lightweight condition.

Wave Drag Characteristics

Supersonic configurations are typically area-ruled to minimize wave drag. The sonic boom constraint adds a competing requirement on the equivalent area, a quantity that is not equal to but is closely related to the physical cross-sectional area. It is, therefore, interesting to review the impact of the sonic boom constraint on the wave drag characteristics of the designs.

Figures 19 and 20 show the cross-sectional area distributions of the two designs. Note that the distributions shown are based on normal cuts; the actual wave drag calculation uses a family of distributions generated by Mach plane cuts at various orientations, and this tends to smooth out the hump that is seen in the normal area distribution of the high-boom aircraft. Important characteristics relative to volume-dependent wave drag are listed in Table 5. The low-boom aircraft is longer, but it also has more volume. Note that the dimensional wave drag, in terms of D/q, is very similar. However, relative to an ideal body of revolution having the same length and volume,

Table 5 Comparison of wave drag characteristics

Characteristic	Low-Boom	High-Boom
Length, ft	165.5	133.5
Volume, ft^3	6030	4500
D (wave)/q, ft^2	8.70	8.50
D (wave)/D (wave)$_{ideal}$	4.4	3.3
Wing area, ft^2	2743	1770
$C_{D(wave)}$	0.0032	0.0048

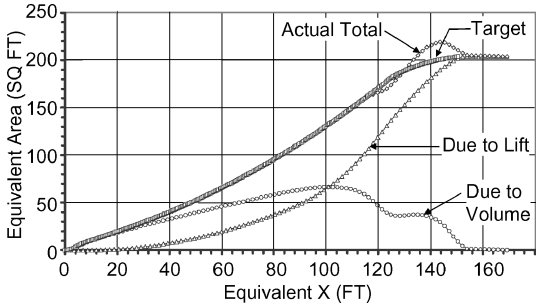

Fig. 21 Low-boom equivalent area distribution.

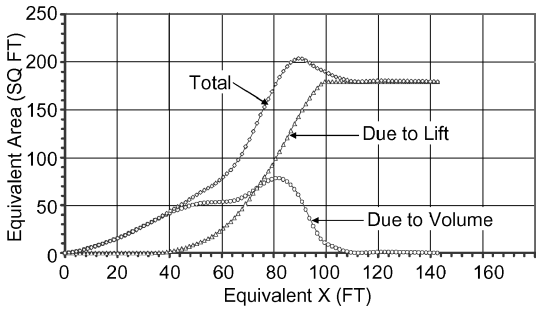

Fig. 22 High-boom equivalent area distribution.

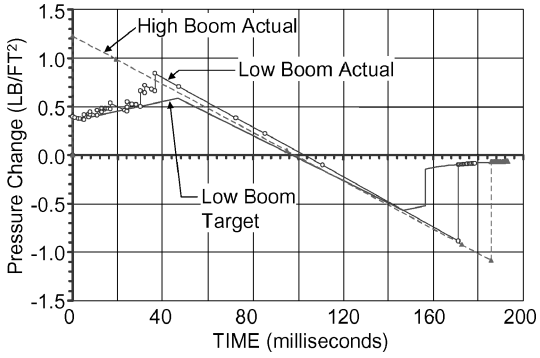

Fig. 23 Sonic boom signatures at initial cruise.

the low-boom aircraft is less efficient. This reflects the compromises to the area ruling imposed by the sonic boom constraint. Because of the larger reference area of the low-boom aircraft, the wave drag coefficient is lower.

Sonic Boom Characteristics

The equivalent area distributions of the two designs are shown in Figs. 21 and 22. The boom signatures of both designs at initial cruise, along with the target for the constrained design, are shown in Fig. 23. The low-boom distribution shows deviations from the target near the aft end. The large hump above the target is due to the nacelle. As a consequence of having to meet stage 4 airfield noise limits, the engines have a higher bypass ratio and a larger diameter than they would if designed solely for the supersonic cruise condition. This made it difficult to keep them within the target equivalent area distribution. They are far enough aft that the initial boom overpressure is not affected; however, the nacelles are responsible for the secondary rise in the boom signature between 30 and 40 ms. The small dip below the target, just ahead of the nacelle, is a concession to wave drag. Approximately three counts of wave drag were saved, with negligible effect on the boom signature, by making this local reduction in the area of the fuselage. The sonic boom overpressures of both designs, throughout the cruise segment of the mission, are listed in Table 6.

Table 6 Sonic boom analysis results

Condition	Weight, lb	Altitude, ft	Initial ΔP, psf
High boom			
Initial cruise	89,100	58,300	1.23
Midcruise	67,900	63,300	1.03
Final cruise	50,600	67,900	0.86
Low boom			
Initial cruise	106,100	57,300	0.40
Midcruise	79,700	62,400	0.33
Final cruise	59,500	66,800	0.29

Conclusions

Two supersonic business aircraft were designed to identical sets of performance requirements, with the single exception of a sonic boom constraint that only applied to one of the aircraft. The present study had two primary objectives: first, the design of these two aircraft and, second, the development of a design process appropriate to the low sonic boom design problem.

Sonic boom reduction introduces unusual physical constraints into the airplane design process. The study focused on understanding the physical significance of the new constraints, rather than on intensive numerical calculations. The result was a process for the intelligent, concurrent management of the various disciplines of boom design, wave drag, volume management, internal layout, and balance.

To solve the problems that arose, it was important to think of the configuration in terms that related to the new constraints, for example, what does a configuration look like on the equivalent area plot? Tools were developed that aided this thought process. Through appropriate simplifications, attention was focused on the fundamental physics of the problem and reasonable solutions were quickly obtained.

The boom-constrained design was approximately 25% longer, with 18% higher takeoff gross weight than the unconstrained design. However, there were also reassuring similarities between the two designs. The boom-constrained aircraft had slightly larger wingspan and engine scaling, commensurate with its higher gross weight, but the only radical differences between the designs are the long nose and wing leading-edge extension on the constrained design. Because of the balance constraint, these components of the constrained vehicle do not contain any major weight items. The nose and leading-edge extension of the constrained aircraft can, therefore, be considered aerodynamic fairings solely to provide the required sonic boom characteristics. The internal arrangements and bulk proportions of the two aircraft are very similar from the cockpit aft.

The boom-constrained aircraft is extremely long, at 165.5 ft. The feasibility of such a large aircraft will have to be assessed in future studies. Relaxing the boom signature target and/or the mission range would allow for a shorter vehicle. For the purposes of this study, both designs are considered to have met the stated performance requirements, which were identical with the exception of the sonic boom requirement for the boom-constrained aircraft.

Acknowledgment

Research sponsored by NASA Langley Research Center, Research Contract L-71387D.

References

[1]Blateau, V., Carreras, C., Chacon, V., Daouk, M., Downen, T., Eremenko, P., Hinton, D., Huber, J., Jamonet, L., Lassaux, G., Lederle, S., Sharkey, J., Sharman, D., and Wertenberg, R., "Beyond the Barrier: The Case for A Practical Small Supersonic Transport," Aircraft Systems Engineering Design Rept. 16.899, Massachusetts Inst. of Technology, Cambridge, MA, May 2001.

[2]Mack, R., and Haglund, G., "A Practical Low-Boom Overpressure Signature Based on Minimum Sonic Boom Theory," *High-Speed Research: Sonic Boom,* NASA CP-3173, Vol. 2, 1992, pp. 15–29.

[3]Alonso, J. J., Kroo, I. M., and Jameson, A., "Advanced Algorithms for Design and Optimization of Quiet Supersonic Platforms," AIAA Paper 2002-0144, Jan. 2002.

[4]Darden, C., "Sonic Boom Minimization with Nose-Bluntness Relaxation," NASA TP-1348, Jan. 1979.

[5]Coen, P., "Development of a Computer Technique for the Prediction of Transport Aircraft Flight Profile Sonic Boom Signatures," M.S. Thesis, School of Engineering and Applied Science, George Washington Univ., Washington, DC, March 1991.

[6]Carlson, H., Walkley, K., Darden, C., Mann, M., and McCullers, A., "Guides to AERO2S and WINGDES Computer Codes for Prediction and Minimization of Drag Due to Lift," NASA TP-3637, Nov. 1997.

[7]Miranda, L., Elliott, R., and Baker, W., "A Generalized Vortex Lattice Method for Subsonic and Supersonic Flow Applications," NASA Contractor Rept. 2865, Dec. 1977.

[8]Harris, R., Jr., "An Analysis and Correlation of Aircraft Wave Drag," NASA TM X-947, March 1964.

[9]McCullers, L., "Aircraft Configuration Optimization Including Optimized Flight Profiles," NASA Technical Reports Server Document ID 19870002310, Jan. 1984.

[10]Hayes, W. D., "Linearized Supersonic Flow," Ph.D. Dissertation, California Inst. of Technology, Pasadena, CA, 1947.

[11]Hayes, W. D., "Linearized Supersonic Flow," Princeton Univ., Department of Aerospace and Mechanical Sciences, AMS Rept. 852, Princeton, NJ, Oct. 1968.

[12]Whitham, G. B., "The Flow Pattern of a Supersonic Projectile," *Communications on Pure and Applied Mathematics,* Vol. 5, No. 3, 1952, pp. 301–348.

[13]Whitham, G. B., "On the Propagation of Weak Shock Waves," *Journal of Fluid Mechanics*, Vol. 1, 1956, pp. 290–317.

[14]Carlson, H. W., and Maglieri, D. J., "Review of Sonic-Boom Generation Theory and Prediction Methods," *Journal of the Acoustical Society of America*, Vol. 51, No. 2, Pt. 3, 1972, pp. 675–685.

[15]Seebass, R., "Sonic Boom Theory," *Journal of Aircraft*, Vol. 6, No. 3, 1969, pp. 177–184.

[16]McLean, F. E., "Some Nonasymptotic Effects on the Sonic Boom of Large Airplanes," NASA TN D-2877, June 1965.

[17]Hayes, W. D., "Brief Review of the Basic Theory," *Sonic Boom Research*, edited by R. Seebass, NASA SP-147, April 1967.

[18]Seebass, R., and George, A., "Sonic Boom Minimization," *Journal of the Acoustical Society of America*, Vol. 51, No. 2, Pt. 3, 1972, pp. 686–694.

[19]Darden, C. M. (ed.), *High-Speed Research: Sonic Boom*, NASA CP-3173, Vol. 2, Feb. 1992.

[20]Mack, R. J., "Some Considerations on the Integration of Engine Nacelles into Low-Boom Aircraft Concepts," *High-Speed Research: Sonic Boom*, NASA CP-3173, Vol. 2, 1992, pp. 221–235.

[21]Nadarajah, S. K., Jameson, A., and Alonso, J. J., "Sonic Boom Reduction Using an Adjoint Method for Wing-Body Configurations in Supersonic Flow," AIAA Paper 2002-5547, Sept. 2002.

[22]Sasaki, D., and Obayashi, S., "Low-Boom Design Optimization for SST Canard–Wing–Fuselage Configuration," AIAA Paper 2003-3432, June 2003.

[23]Chung, H.-S., Choi, S., and Alonso, J. J., "Supersonic Business Jet Design Using a Knowledge-Based Genetic Algorithm with an Adaptive, Unstructured Grid Methodology," AIAA Paper 2003-3791, June 2003.

[24]Boccadoro, C., Graham, D., Maglieri, D., Coen, P., and Pawlowski, J., "Origins of the Shaped Sonic Boom Demonstration Program," AIAA Paper 2005-0005, Jan. 2005.

[25]Sweetman, B., "Whooshhh! The Next Generation of Supersonic Aircraft," *Popular Science*, Vol. 265, No. 1, 2004, pp. 56–62.

[26]Choi, S., and Alonso, J., "Multi-Fidelity Design Optimization of Low-Boom Supersonic Business Jet," AIAA Paper 2004-4371, Aug. 2004.

[27]Baize, D., and Coen, P., "A Mach 2.0/1.6 Low Sonic Boom High-Speed Civil Transport Concept," *High Speed Research: Sonic Boom*, NASA CP-10133, Vol. 2, 1993, pp. 125–142.

[28]Wolz, R., "A Summary of Recent Supersonic Vehicle Studies at Gulfstream Aerospace," AIAA Paper 2003-0558, Jan. 2003.

[29]Hartwich, P., Burroughs, W., Herzberg, J., and Wiler, D., "Design Development Strategies and Technology Integration for Supersonic Aircraft of Low Perceived Sonic Boom," AIAA Paper 2003-0556, Jan. 2003.

[30]Mack, R. J., "An Analysis of Measured Sonic-Boom Pressure Signatures from a Langley Wind-Tunnel Model of a Supersonic-Cruise Business Jet Concept," NASA TM-2003-212447, Oct. 2003.

[31]Howe, D., "Sonic Boom Reduction Through the Use of Non-Axisymmetric Configuration Shaping," AIAA Paper 2003-0929, Jan. 2003.

[32]Maglieri, D., "Sonic Boom Flight Research—Some Effects of Airplane Operations and the Atmosphere on Sonic Boom Signatures," NASA SP-147, Jan. 1967.

[33]Hilton, D., Huckel, V., Steiner, R., and Maglieri, D., "Sonic-Boom Exposures During FAA Community-Response Studies over a 6-Month Period in the Oklahoma City Area," NASA TN D-2539, Dec. 1964.

[34]Hubbard, H., Maglieri, D., Huckel, V., and Hilton, D., "Ground Measurements of Sonic-Boom Pressures for the Altitude Range of 10,000 to 75,000 Feet," NASA TR R-198, July 1964.

[35]"Sonic Boom Experiments at Edwards Air Force Base," Rept. NSBEO-1-67, CFSTI, U.S. Dept. of Commerce, July 1967.

[36]Torenbeek, E., "Airplane Weight and Balance," and "Appendix C: Prediction of Wing Structural Weight," *Synthesis of Subsonic Airplane Design*, Delft Univ. Press, Delft, The Netherlands, 1982, Chap. 8, pp. 263–302, and 451–456.

[37]Roskam, J., *Airplane Design, Part V: Component Weight Estimation*, Roskam Aviation and Engineering Corp., Ottawa, KS, 1989.

[38]Raymer, D., "Fuel System," *Aircraft Design: A Conceptual Approach*, 3rd ed., AIAA, Reston, VA, 1999, Sec. 10.5, pp. 267–270.

[39]"Special Conditions for the Societe Nationale Industrielle Aerospatiale/British Aircraft Corporation Concorde Model Airplane," Federal Aviation Administration, Dept. of Transportation, Docket 10068, Special Conditions 25-43-EU-12, July 1973.

[40]"Noise Standards: Aircraft Type and Airworthiness Certification," Federal Aviation Administration, Dept. of Transportation, Advisory Circulary AC 36-4C, July 2003.